Design and Analysis of Two-Degree-of-Freedom Voice Coil Motors for Linear-Rotary Motion

Zi-jiao Zhang[1,2], Hai-bo Zhou[1,2], Ji-an Duan[1,2] and Bao-quan Kou[3]
[1]State Key Laboratory of High Performance Complex Manufacturing, Central South University, Changsha, 410083, China
[2]School of Mechanical and Electrical Engineering, Central South University, Changsha, 410083, China
[3] School of Electrical Engineering and Automation, Harbin Institute of Technology, Harbin, 150001, China
E-mail: xinruoliuli.07@163.com

***Abstract*—As the development of precise machining, electrical machines with high precision and high dynamic are the focus of research. This paper proposes three kinds of two-degree-of-freedom Voice Coil Motor (VCM), which provide linear-rotary motion. The VCM with two motion units has a great controllability and perfect rotary torque features, the one with parallel axes of motions has the highest average linear thrust, and the one with vertical axes of motions has the lowest thrust ripple and the highest average rotary torque. Structures of three VCMs are introduced firstly, and the magnetic circuits of three motors are analyzed. Then force features of three motors are calculated and compared by finite-element-method (FEM), and a prototype is machined and tested for performance verification. The paper provides the fundamental work for the two-degree-of-freedom VCMs, accomplishes the basic performance analyses.**

***Index Terms*-- Two-degree-of-freedom motor, Voice Coil Motor (VCM), linear thrust, rotary torque.**

I. Introduction

Precise machining has the requirements of running stability and quick response for motion units, so electrical machines with low thrust ripple and high dynamic performance are popular in multidimensional precision motion platform, and Voice Coil Motor (VCM) has more advantages of small size and high controllability which is one of the best choices for multidimensional platform.

Error accumulation coming from motion-superposition is always the difficulty for multidimensional precision motion platform, and the problem can be solved by the multi-degree-of-freedom motors, because intermediate components for the connections and converts of different dimensional motion are avoided. Thus, the VCM with two-degree-of-freedom has these excellent performances of VCM and eliminates the accumulative error of two different dimensional motions. And the size of motor are reduced, because the two motions share the magnetic field in two-degree-of-freedom VCM.

The researches of VCM are concentrated in rotary VCM, which are widely used in optical disk drives and hard disk drives [1]. Lee *et al*. [2] design and optimize a rotary VCM for high dynamic performance. In [3], Chou *et al*. propose a novel rotary VCM for seesaw swing arm actuator which is adopted in optical disk drive. In [4] Cao *et al*. design a novel high-precision swing-arm VCM and the simulation are accomplished by the Maxwell 2D of Ansoft. In terms of linear VCM, the focus is high linear thrust. Lou *et al*. [1] develop a linear VCM to improve the force constant. In [5], the authors give an engineering procedure which is established on a statistic model to optimize a linear VCM for subminiature optical storage devices. However, there are few literatures involving two-degree-of-freedom VCM, so the design methods and optimization directions of this kind motor need to be studied detailedly.

In this paper, three kinds of two-degree-of-freedom VCMs are proposed here: the one with two independent magnetic fields for two motions units respectively has perfect rotary torque features and a great controllability, due to the independent magnetic circuits in two motion units and its radial magnetic field in rotary motion unit; the one with parallel axes of motions has a high linear thrust, due to its bilateral magnetic excitations; and the one with vertical axes of motions has a low thrust ripple and a high rotary torque, for its large radius of rotary motion. High average force helps to reduce the motor size, and low force ripple helps to improve the running precision of VCM, so designs and analyses are proceeded with the both goals. Parameter optimizations of three novel VCMs and prototype test are accomplished here.

II. Structures of Two-Degree-of-Freedom VCMs

For the requirement of high dynamic performance in precise machining, three kinds of two-degree-of-freedom VCMs all adopt the moving coil type and coreless structure, permanent magnets are fastened on iron yokes. The linear guides and sliders make the motor movers running along the designed tracks, and the outputs of synthetic motions are the terminals of the linear-rotary motions in three two-degree-of-freedom VCMs.

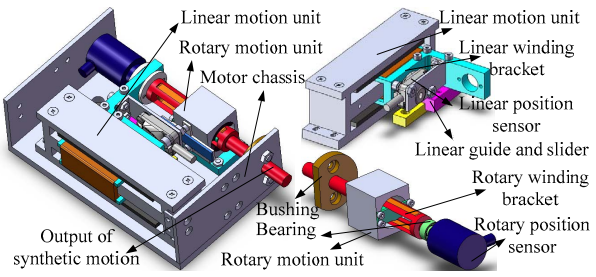

Fig. 1. VCM with two motion units.

The two-degree-of-freedom VCM shown in Fig. 1, has two independent motion units. The linear motion unit is a

This work was supported in part by the National Natural Science Foundation of China under Grant 51575534 and the Natural Science Foundation of Hunan Province of China under Grant 2015JJ4078, and in part by Self-selected Topic Fund of State Key Laboratory of High Performance Complex Manufacturing under Grant ZZYJKT2015-10.

bilateral motor and has magnetic circuits in parallel. The rotary motion unit has similar magnetic circuit structure to the linear motion unit. The rotary winding bracket is fixedly connected with the linear winding bracket. The rotary winding is long enough for that part of rotary winding always suspends in the magnetic field of the rotary motion unit, when the rotary winding moves with the linear winding.

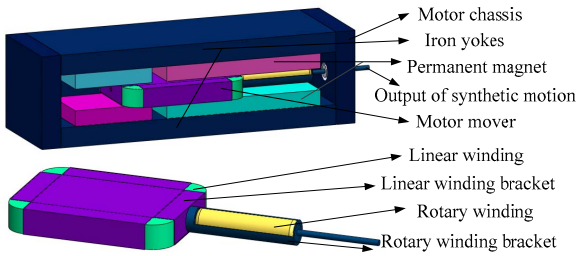

Fig. 2. VCM with parallel axes of linear and rotary motions.

VCM shown in Fig. 2, has a brief structure, and two pairs of permanent magnets. The magnetic field which is excited by the pair of smaller permanent magnets, is only used to generate the Lorenz force with one side of linear winding. And the magnetic field excited by the other pair of larger permanent magnets, interacts with rotary winding and the other side of linear winding for linear thrust and rotary torque. The utilizations of linear and rotary windings are high, and the bilateral magnetic excitations are adopted in this motor, so the linear thrust density are improved, but the rotary torque is low for the small radius of rotary motion.

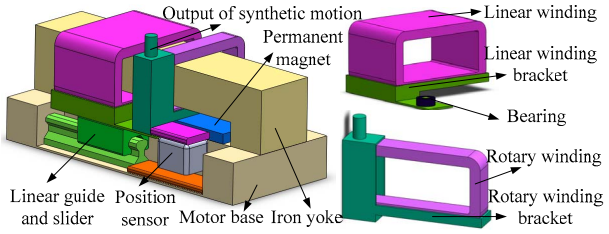

Fig. 3. VCM with vertical axes of linear and rotary motions.

The axes of linear motion and rotary motion in the two-degree-of-freedom VCM shown in Fig. 3, are perpendicular. Both of linear winding and rotary winding have one single side to generate the Lorenz force for linear-rotary motion. The radius of rotary motion in this motor is nearly long as the axial length of rotary winding. Thus the motor has an advantage of rotary torque over the other two motors, which can provide a higher rotary torque with the same current and a low torque ripple.

VCM is well known for its capabilities in running precision and fast response, so the force performances are emphatically analyzed in this paper. Optimal designs of three two-degree-of-freedom VCMs are proceeded and compared to demonstrate their applicabilities.

III. Magnetic Circuit Analyses of Two-Degree-of-Freedom VCMs

Magnetic flux lines in three two-degree-of-freedom VCMs, excited by permanent magnets, are closed curves, getting through the mechanical air-gaps and coils, shown in Fig. 4. When the residual magnetic flux density of permanent magnet is B_r and the magnetization length of permanent magnet is h_m, the magnetomotive force F_m of permanent magnet can be given by

$$F_m = \frac{B_r h_m}{\mu_r \mu_0} \tag{1}$$

where μ_r is the relative magnetic permeability of permanent magnet and μ_0 is the permeability of vacuum.

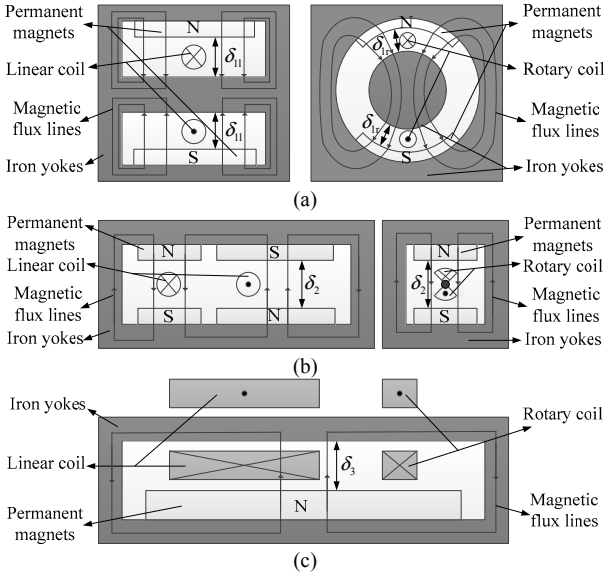

Fig. 4. Magnetic circuits in two-degree-of-freedom VCMs, (a) motor with two motion units(Model I), (b) motor with parallel axes of motions(Model II), (c) motor with vertical axes of motions(Model III).

The magnetic circuit models shown in Fig. 4, are noted as Model I, Model II and Model III. The magnetic flux densities of air-gaps in linear motion unit and rotary motion unit of Model I are $B_{1\delta l}$ and $B_{1\delta r}$, and the magnetic flux densities of air-gap in Model II and Model III are named after $B_{2\delta}$ and $B_{3\delta}$. μ_{Fe} is the relative magnetic permeability of iron yoke, H_{Fe} is the magnetic intensity of iron yoke, and the average lengths of magnetic flux lines in the iron yokes for the three model are noted as l_{1Fel}, l_{1Fer}, l_{2Fe} and l_{3Fe}. Then the magnetic densities of air-gaps in three models are given by

$$\begin{cases} B_{1\delta l} = \dfrac{B_r h_m}{\mu_r \delta_{1l}} - \dfrac{\mu_0 H_{Fe} l_{1Fel}}{\delta_{1l}} \\ B_{1\delta r} = \dfrac{B_r h_m}{\mu_r \delta_{1r}} - \dfrac{\mu_0 H_{Fe} l_{1Fer}}{2\delta_{1r}} \end{cases} \tag{2}$$

$$B_{2\delta} = \frac{2B_r h_m}{\mu_r \delta_2} - \frac{\mu_0 H_{Fe} l_{2Fe}}{\delta_2} \tag{3}$$

$$B_{3\delta} = \frac{B_r h_m}{\mu_r \delta_3} - \frac{\mu_0 H_{Fe} l_{3Fe}}{\delta_3} \tag{4}$$

where δ_{1l} and δ_{1r} are the lengths of mechanical air-gaps in the linear motion unit and the rotary motion unit of Model I, δ_2 and δ_3 are the lengths of mechanical air-gaps in Model II and Model III.

Lorenz force is generated by the effect of magnetic field on electrified conductor, so $F=NB_{\delta}Il_{m}$, where N is the number of turns in coil, I is the current in conductors, B_{δ} is the magnetic flux density of air-gap, and l_{m} is the length of permanent magnet in axial direction. The surface current density and the axial length of permanent magnet in three models take the similar values, to clear the analyses and comparisons of three VCMs.

Then the magnetic flux density B_{δ} of air-gap is the main parameter influencing Lorenz force F. According to (2)-(4) and the practical application of VCM, the parameters which are constant in the following analyses, are shown in Table I.

TABLE I
PARAMETERS OF TWO-DEGREE-OF-FREEDOM VCMS

Parameter	Model I	Model II	Model III
Linear stroke	20 mm	20 mm	20 mm
Rotary stroke	30°	30°	30°
Axial length of permanent magnet	50 mm	50 mm	50 mm
Surface current density for linear motion	9 A/mm^2	9 A/mm^2	9 A/mm^2
Surface current density for rotary motion	10.4 A/mm^2	9 A/mm^2	10.2 A/mm^2

IV. PERFORMANCE OPTIMIZATIONS OF TWO-DEGREE-OF-FREEDOM VCMS

Magnetic field of VCM effects Lorenz force in three ways: magnetic excitation, magnetic saturation and armature reaction. The influences of these aspects on the linear thrust and the rotary torque in three kinds of two-degree-of-freedom VCMs are similar, so the variations of linear thrust are taken as examples. In the magnetic excitation of VCM, the magnetization length h_{m} of permanent magnet is the most important factor according to (1), and the mechanical air-gap δ is also the key. For the magnetic saturation in VCM, the thickness h_{j} of iron yoke is the main parameter, and other two parameters are taken into considerations which are the distance $d_{m\text{-}w}$ from the edge of coil in the initial position to the edge of permanent magnet and the distance $d_{j\text{-}m}$ from the edge of permanent magnet to the edge of iron yoke. In terms of the armature reaction in VCM, only the ratio b_{w}/h_{w} are studied due to the space limitation, where b_{w} is the width of coil and h_{w} is the thickness of coil.

For the rotary motions in the three VCMs, the cross-sections of rotary coils are analyzed here, which are related to the armature reactions in rotary windings.

A. Magnetization Length h_{m} of Permanent Magnet

Magnetomotive force F_{m} increases as magnetization length h_{m} of permanent magnet grows, before magnetic saturation occurs. The variations of linear thrust with h_{m} are taken as examples which are shown in Fig. 5.

Data in Fig. 5(a) show that all of curves are saturated when h_{m} is higher than a certain value, and the average thrust of Model II is higher than others for permanent magnets on the both sides of coil exciting the magnetic field in Model I. The influences of h_{m} match with the magnetization curve of iron Thus the magnetization lengths in three models could be taken as 8 mm, 4 mm and 8 mm when linear thrusts are set as 8 N.

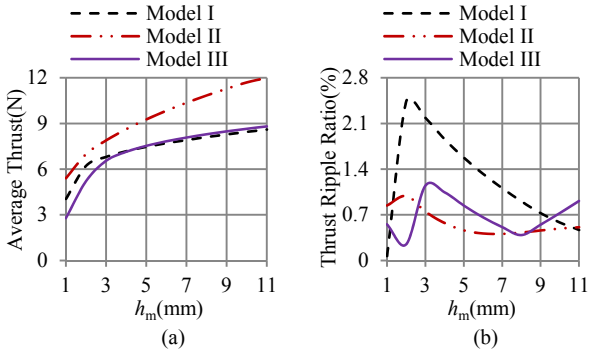

Fig. 5. Variations of linear thrust with h_{m}, (a) average thrust, (b) thrust ripple ratio.

Fig. 5(b) shows that the thrust ripple ratio of Model III is 0.39% which is lower than other two, when the magnetization lengths of permanent magnets in three models could be taken as 8 mm, 4 mm and 8 mm.

B. Mechanical Air-gap δ

Mechanical air-gap δ is always the main factor for force characteristics in all kinds of motors. The reluctance of magnetic circuit increases and the magnetic flux density decrease as the mechanical air-gap grows, when the magnetic excitation is constant. Fig. 6 shows the variations of linear thrust with δ in the three VCMs.

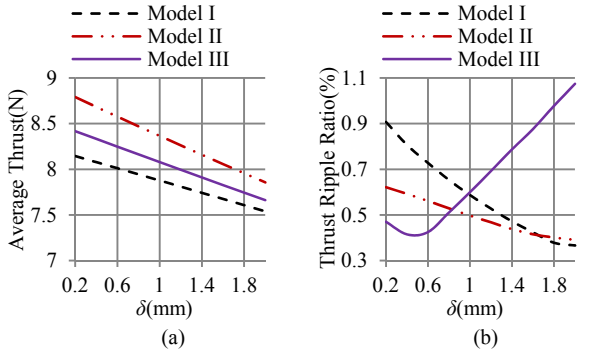

Fig. 6. Variations of linear thrust with δ, (a) average thrust, (b) thrust ripple ratio.

The average thrusts in Fig. 6(a) decline with a raise of δ, which conforms to the theory. Data in Fig. 6 show that δ should be set as 0.6 mm, 1.8 mm and 0.5 mm in Model I, Model II and Model III respectively, when linear thrusts are set as 8 N and thrust ripple ratios are reduced as possible. And the thrust ripple ration in Model III is the lowest one (0.38%).

C. Thickness h_{j} of Iron Yoke

Magnetic saturation in VCM is more likely to happen, because VCM usually takes relatively thin iron yoke for small size and light weight.

Curves in Fig. 7 show the influences of h_{j} on linear thrust of three VCMs, which match with the magnetization curve of iron. When h_{j} increases to a particular point, the magnetic saturations happen, and the linear thrust ripple decline obviously. Data in Fig. 7 show that magnetic saturations occur when h_{j} is 9 mm in Model I and Model III, and magnetic saturation begins when h_{j} is 5 mm in Model II. The reason is the bilateral magnetic excitations are adopted in Model II.

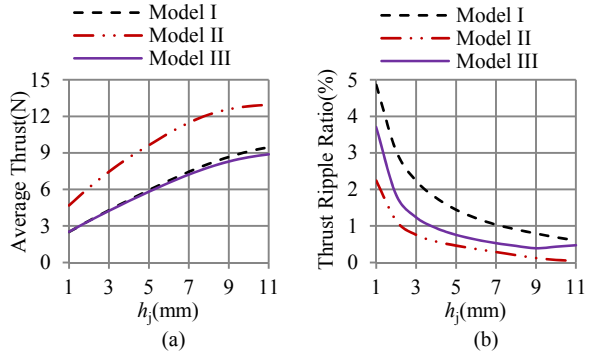

Fig. 7. Variations of linear thrust with h_j, (a) average thrust, (b) thrust ripple ratio.

D. Distance $d_{m\text{-}w}$ and $d_{j\text{-}m}$

The distance $d_{m\text{-}w}$ from the edge of coil in the initial position to the edge of permanent magnet should be chosen as a suitable value. The magnetic field distortion increases when $d_{m\text{-}w}$ is too short, and the space is wasted when $d_{m\text{-}w}$ is too long. Fig. 8 shows $d_{m\text{-}w}$ should be 6 mm in Model I and II, and $d_{m\text{-}w}$ should be 10 mm in Model III

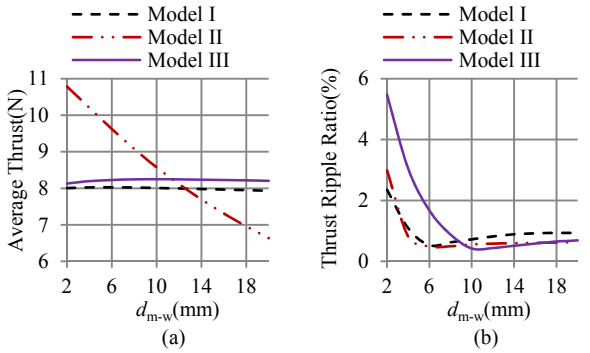

Fig. 8. Variations of linear thrust with $d_{m\text{-}w}$, (a) average thrust, (b) thrust ripple ratio.

The distance $d_{j\text{-}m}$ from the edge of permanent magnet to the edge of iron yoke is related to magnetic flux leakage, so $d_{j\text{-}m}$ should be large enough. But the size and weight of VCM increase when $d_{j\text{-}m}$ is too large.

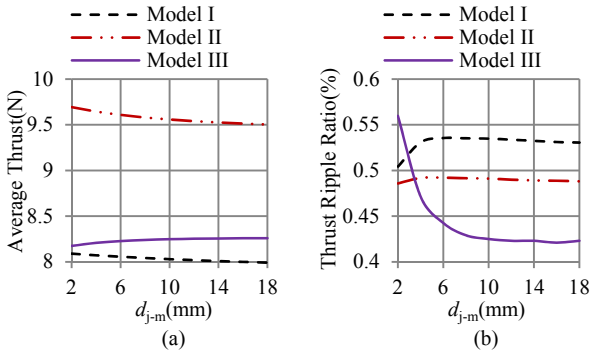

Fig. 9. Variations of linear thrust with $d_{j\text{-}m}$, (a) average thrust, (b) thrust ripple ratio.

E. Ratio b_w/h_w

The equivalent air-gap is the sum of the mechanical air-gap δ, the magnetization length h_m of permanent magnet and the thickness h_w of coil. Thus equivalent air-gap grows as h_w increase, and the width b_w decreases, because the cross-sectional area of coil is constant. So the armature reaction weakens as the ratio b_w/h_w grows.

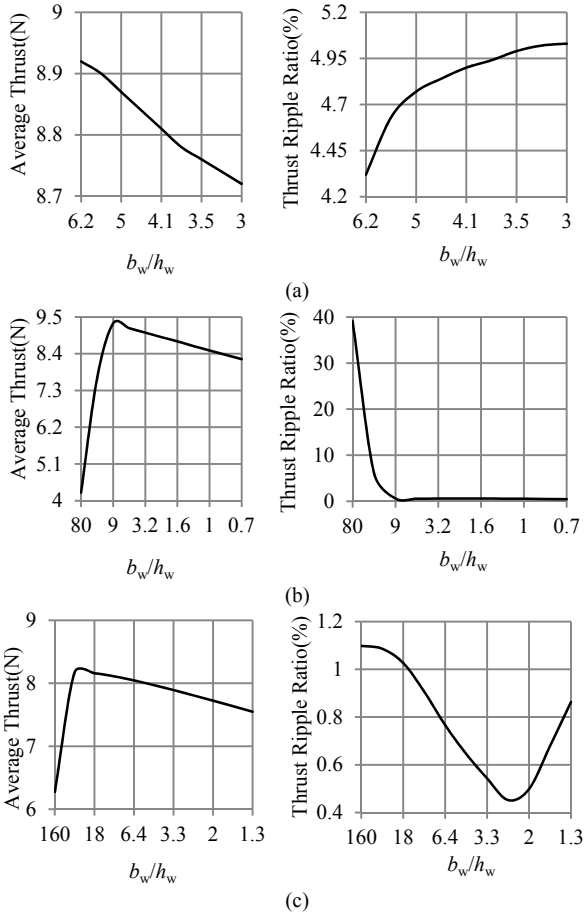

Fig. 10. Variations of linear thrust with b_w/h_w, (a) Model I, (b) Model II, (c) Model III.

Curves in Fig. 10(a) demonstrate that the magnetic field in Model I mainly reflects the increasement of equivalent air-gap when the ratio b_w/h_w grows, instead of the armature reaction. The variations of lineat thrusts in Model II and Model III are mainly affected by the armature reactions when the ratio b_w/h_w is low, and more reflect the increasement of equivalent air-gap when the ratio b_w/h_w is high. The impact of armature reaction in Model II is the most one of three.

F. Cross-Section of Rotary Coil

The cross-sections of rotary coils in three VCMs, affect the armature reactions, which are related to the rotary motion tracks and positions of rotary windings in three motors. Three kinds of VCMs are analyzed respectively, because three rotary models have different electromagnetic structures and different magnetic flux lines, which are shown in Fig. 11.

Curves in Fig. 11 demonstrate that the torque performances in Model I and Model III are better than the ones in Model II, regarding of the average torques and torque ripple ratios. The magnetic flux lines are parallel in the air-gap of Model II, which is the reason of the large torque ripple ratio. Model I has a perfect torque ripple ratio, for its radial magnetic excitation. And Model III is excellent in a high average torque, due to the large radius of rotary motion.

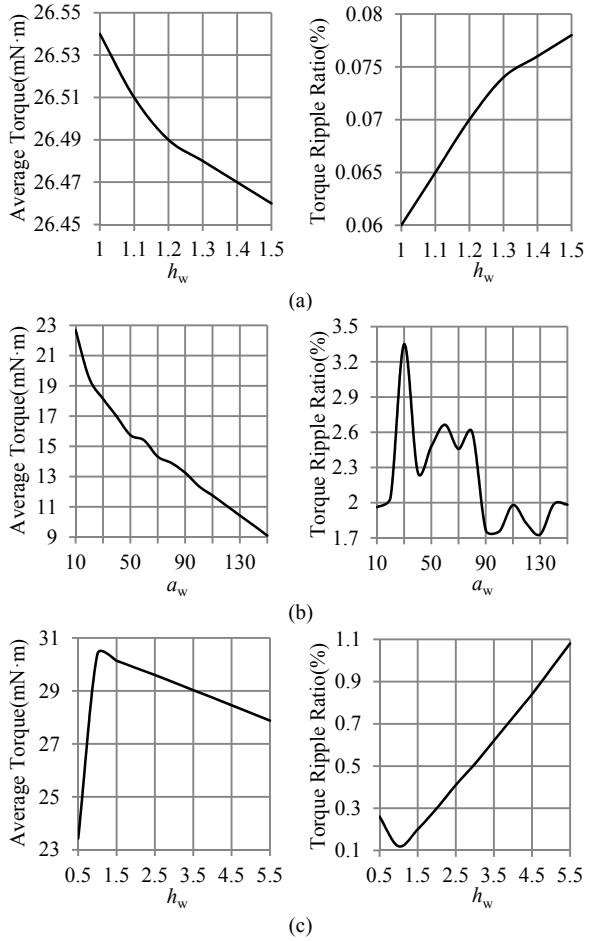

Fig. 11. Variations of rotary torques with the cross-secitons of rotary coils, (a) Model I, (b) Model II, (c) Model III.

Performances of three two-degree-of-freedom VCMs are shown in Table II, which are optimized by the finite-element-method (FEM).

TABLE II
PERFORMANCES OF TWO-DEGREE-OF-FREEDOM VCMS

Performance	Model I	Model II	Model III
Length (mm) × height (mm) × width (mm)	100×34×66	180×24×50	102×35×57
Volume (mm^3)	224400	216000	203490
Average linear thrust (N)	8.02	9.42	8.25
Thrust ripple ratio (%)	0.53	0.49	0.38
Average rotary torque (mN·m)	26.54	12.37	30.39
Torque ripple ratio (%)	0.06	1.76	0.12

V. PROTOTYPE TEST

In order to verify the performances of VCM with two-degree-of-freedom, a prototype for Model I is designed and tested shown in Fig. 12.

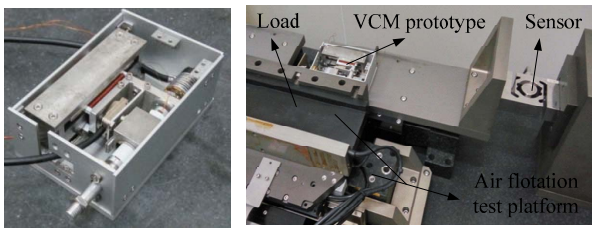

Fig. 12. Prototype for Model I, (a) prototype, (b) test platform.

The experiments for the linear thrust and rotary torque of the two-degree-of-freedom VCM shown in Fig. 12, have been done. The force features of this prototype are shown in Fig. 13. The features of rotary torque from experiment can match up with the ones from simulations, which is shown in Fig. 13(b).

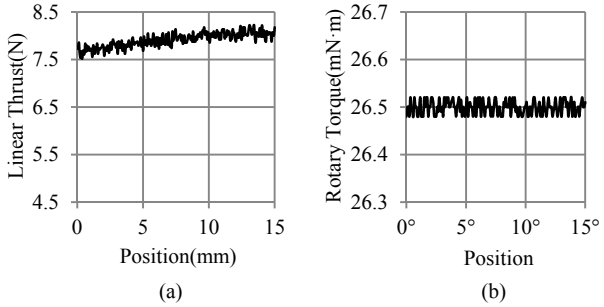

Fig. 13. Force features of the prototype, (a) linear thrust, (b) rotary torque.

For the stationarity of linear motion, the suitable stroke of linear motion in this motor is the range from 10 mm to 15 mm in Fig. 13(a), the average linear thrust is 8 N and the thrust ripple ratio is 1.1%. The average linear thrusts from the simulation and experiment are consistent, but the difference of the thrust ripple ratios from the simulation and experiment is significant which mainly came from the test platform. And it can be seen that the basic designs of the two-degree-of-freedom VCMs are demonstrated. The prototypes for Model II and Model III are in processing manufactures now, the experimental tests of the two VCMs will be proceeded when the machining of prototypes is accomplished.

VI. CONCLUSIONS

The analyses and calculations indicate the following.

1) Structure analyses of three two-degree-of-freedom VCMs demonstrate that three proposed linear-rotary motors can effectively satisfy for multidimensional precision motion platform, which are characterized by running stability and quick response.

2) For the linear thrusts of three motors, the influences of h_m and h_j match with the magnetization curve of iron, δ mainly acts on the reluctance of magnetic circuit, the impact of b_w/h_w comes from the change of equivalent air-gap and the armature reaction, and the actions of $d_{m\text{-}w}$ and $d_{j\text{-}m}$ are related to the magnetic field distortion and magnetic flux leakage.

3) In terms of the rotary torque, the main differences of three VCMs come from the different magnetic circuit structures. VCM with two motion units has a perfect torque ripple ratio, for its radial magnetic excitation. And VCM with vertical axes of motions is excellent in a high average torque, due to the large radius of rotary motion.

4) Performances of three two-degree-of-freedom VCMs in Table II are compared: VCM with two motion units (Model I) has great features of rotary torque (the torque ripple ratio is 0.06%); VCM with parallel axes of two motions (Model II) has a highest linear thrust (9.42 N), but its rotary torque is unsatisfactory; VCM with vertical axes of two motions (Model III) has a lowest

linear thrust ripple ratio (0.38%) and a highest rotary torque (30.39 mN·m).

5) A prototype for the VCM with two motion units are machined and tested. The average linear thrust is 8 N and the thrust ripple ratio is 1.1%, the error of the thrust ripple ratios from the simulation and experiment is significant which mainly came from the test platform. And the features of rotary torque from experiment can match up with the ones from simulations. So the basic designs of the two-degree-of-freedom VCMs are verified.

REFERENCES

[1] Yun-jiang Lou, Xian-sheng Yang, Ke Li, and *et al*. "Design and optimization of a linear voice coil motor for LED die bonders," *International Conference on Information and Automation*, *ICIA*., pp. 1011-1016, Aug. 2013.

[2] H.-S. Lee, Y.-H. Kim, T.-Y. Hwang, and *et al*. "VCM design to improve dynamic performance of an actuator in a disk drive," *IEEE Trans. Magn.*, vol. 41, no. 2, pp. 774–778, Feb. 2005.

[3] Po-Chien Chou, Yu-Cheng Lin, and Stone Cheng. "A novel seesaw swivel actuator design and fabrication," *IEEE Trans. Magn.*, vol. 46, no. 7, pp. 2603–2610, Mar. 2010.

[4] Yong-hui Cao, Shuai Wu, and Zong-xia Jiao. "Design and simulation of Voice Coil Motor for the micro-electric load simulator," *International Conference on Fluid Power and Mechatronics*, *ICFPM*., pp. 930-934, Aug. 2011.

[5] D.-J. Lee, K.-S. Woo, N.-C. Park, and Y.-P. Park. "Design and optimization of a linear actuator for subminiature optical storage devices," *IEEE Trans. Magn.*, vol. 41, no. 2, pp. 1055–1057, Feb. 2005.

[6] Chih-min Lin, and Hsin-yi Li. "Voice coil motor motion control using fuzzy cerebellar model articulation controller," 2011 IEEE International Conference on System Science and Engineering, ICSSE'11., pp. 264-269, Jun. 2011.

[7] Chih-Min Lin, and Hsin-Yi Li. "A novel adaptive wavelet fuzzy cerebellar model articulation control system design for Voice Coil Motors," IEEE Trans. Ind. Electron., vol. 59, no. 4, pp. 2024–2033, Jun. 2011.

[8] Kemao Peng, B. M. Chen, Guoyang Chen, and T. H. Lee. "Modeling and compensation of nonlinearities and friction in a micro hard disk drive servo system with nonlinear feedback control," IEEE Trans. Control Syst.Technol., vol. 13, no. 5, pp. 708–721, Sep. 2005.

[9] R. Oboe, A. Beghi, P. Capretta, and F. C. Soldavini. "A simulation and control design environment for single-stage and dual-stage hard disk drives," IEEE/ASME Trans. Mechatronics, vol. 7, no. 2, pp. 161–170, Jun. 2002.

[10] Jungyul Perk, Sangmin Kim, Deok-Ho Kim, and et al. "Advanced controller design and implementation of a sensorized microgripper for micromanipulation," 2004 IEEE International Conference on Robotics and Automation, ICRA'04., pp. 5025-5032, Apr. 2004.